ACCSCIENCE PUBLISHING

International Journal of Bioprinting

RESEARCH ARTICLE

# A new solution for *in situ* monitoring of shape fidelity in extrusion-based bioprinting via thermal imaging

**Simone Giovanni Gugliandolo[1,2], Egon Prioglio[1], Davide Moscatelli[2], and Bianca Maria Colosimo[1]***

[1]Department of Mechanical Engineering, Politecnico di Milano, Via La Masa, 1, 20156, Milano, Italy

[2]Department of Chemistry, Materials and Chemical Engineering "Giulio Natta", Politecnico di Milano, Piazza Leonardo da Vinci, 32, 20133, Milano, Italy

## Abstract

Bioprinting is an interdisciplinary study field, where additive manufacturing is combined with tissue engineering and material sciences. The ever-increasing need for personalized medicine fueled interest in the possibility of using this technique to reproduce biological tissues, allowing bioprinting to establish itself as one of the most promising approach in biomedical research. Producing bioconstructs that resemble living tissues is a very complex and multi-step procedure. Given the complexity of the processes involved, the literature still lacks robust solutions for monitoring the bioprinted construct quality, especially *in situ* and in-line. Here, a novel non-destructive approach for monitoring the geometries of bioprinted constructs based on infrared (IR) imaging is proposed. Besides the intuitive use of IR information to gain insight on the temperature signature, we propose IR video imaging as a viable solution to overcome traditional problems of visible-range imaging for geometry reconstruction with transparent bioinks, especially when precise information on the last printed layer only is required. The results obtained show a significant new direction for in-line monitoring of bioprinting processes.

***Keywords:*** Additive manufacturing; 3D bioprinting; Thermal imaging; Monitoring

***Corresponding author:**
Bianca Maria Colosimo
(biancamaria.colosimo@polimi.it)

**Citation:** Gugliandolo SG, Prioglio E, Moscatelli D, Colosimo BM. A new solution for *in situ* monitoring of shape fidelity in extrusion-based bioprinting via thermal imaging. *Int J Bioprint*. 2024;10(3):2021. doi: 10.36922/ijb.2021

**Received:** October 12, 2023
**Accepted:** December 28, 2023
**Published Online:** March 22, 2024



## 1. Introduction

Bioprinting is an additive manufacturing (AM) technology whose goal is to fabricate parts that mimic the functionality of real tissues and organs by combining cells and biomaterials with a specific three-dimensional (3D) spatial organization. As in traditional AM, the goal is achieved with the use of computer-aided design (CAD) to generate 3D models of the geometry of the tissue or organ of interest to produce bioconstructs that have many applications in regenerative medicine, tissue engineering, reconstructive surgery, drug discovery, pharmacokinetics, food sector, and basic medical and cell biology research.[1,2] Thus, one of the main challenges is to avoid the death of living cells during the printing process. In light of these numerous applications and due to the increasing interest especially in personalized medicine, bioprinting has attracted attention in recent years from both academia and industry.[3] During the last decade, many new techniques and

technologies related to bioprinting have emerged in the state of the art, from specific 3D printers, the bioprinters, to specific soft biomaterials in which living cells can be embedded, called bioinks.[4,5]

Although the bioprinting literature does not typically use the specific terminology defined in AM standards (ISO/ASTM 52900:2021), technologies similar to those used for polymers are often employed. We can identify two main classes of bioprinting technologies:[3] laser-assisted bioprinting and laser-free bioprinting, each of which includes several sub-categories. There are also hybrid technologies or those with particular processes like melt electrowriting (MEW),[6] magnetic 3D cell culture,[7] acoustic assembly,[8] microneedle array,[9] and single-cell printing[10] among the most known.

Laser-free bioprinting offers varying resolutions and speeds influenced by factors like bioprinting head precision, material extrusion mechanisms, nozzle types, and droplet formation methods. Extrusion-based bioprinting (EBB) is widely studied and known for its affordability and compatibility with various biomaterials.[11] In EBB, the impact of mechanical forces, particularly shear stress, on cells and bioink properties must be properly mitigated to preserve cell viability and structural integrity.[12] Inkjet bioprinting is suitable for smaller features but requires low-viscosity biomaterials.[13] Higher viscoelasticity stabilizes droplets, reducing displacement, while increased viscosity improves accuracy and enhances cell viability and proliferation. This highlights the crucial role of bioink properties in optimizing precision and creating tunable cell spheroids.[14] Laser-assisted bioprinting notably utilizes vat photopolymerization methods such as stereolithography (SLA) and digital light processing (DLP). In this sophisticated approach, light serves as the catalyst to either initiate photopolymerization reactions or generate controlled heat and pressure, enabling the precise and intricate fabrication of 3D structures.

Stereolithography and DLP contribute significantly to the refinement and efficacy of laser-assisted bioprinting. These vat photopolymerization techniques excel in providing a higher resolution during the bioprinting process, ensuring the creation of detailed and complex structures with higher precision. The ability to precisely control the initiation of photopolymerization reactions through light-based technologies enhances the accuracy of the deposited bioink materials. One notable advantage of vat photopolymerization methods, particularly SLA and DLP, is their broader compatibility with a diverse range of bioinks.[15] Two-photon polymerization (2PP) achieves nanoscale detail using laser-induced photopolymerization.[16-19] Volumetric bioprinting constructs free-form structures inspired by optical tomography but is limited to photo-curable bioinks and can potentially cause cell damage.[18]

The bioprinting literature is rich with articles studying the bioprinting process capabilities, the development and classification of novel biomaterials, and a specific focus on the tissue of interest.[5,20,21] However, few studies have been investigating solutions for *in situ* monitoring and inspection of bioprinted constructs, as the ones observed in the literature on more conventional AM processes.[22-27] In fact, a few papers mostly from the same research groups have been presented inspecting the quality of the printed construct, detecting defects as well as tools to control and correct deposition errors *in situ*.[28-42]

The lack of repeatability, process stability, and error detection and monitoring in bioprinting represent key technological barriers to the development of products of increasing complexity, especially when hard-to-print biomaterials are involved and the shape fidelity layer-wise can then affect the capability of printing multilayer constructs.[28] Indeed, the industrial repeatability and reproducibility of the printing process is still far from being reached, especially in EBB.[43]

On the other side, the growing advance of non-destructive sensors could bring a significant impact on the development of new solutions for in-line inspection, monitoring, and control in bioprinting.[34] Among non-destructive and non-invasive methods for quality inspection, the most used solutions are image-based methods, which are perceived as time- and cost-effective approaches. In the context of bioprinting, image-based methods could potentially streamline processes by offering precise visualization and automation. This might enhance planning accuracy, reduce the likelihood of errors, and theoretically minimize material wastage, potentially contributing to cost savings. Real-time monitoring might ensure quality control, allowing for quick adjustments and potentially minimizing trial-and-error iterations. It is important to note that the actual efficiency gains would depend on various factors, including tissue complexity and the sophistication of the imaging technologies and data mining approach. Usually, data analysis of the last layer can be done in masked time, while the process is printing the new layer. Once the data mining algorithm is also defined, different solutions to reduce the computational time can be considered by extracting just the relevant features and acting on them. *In situ* monitoring and control via image-based analysis can bring advantages, which are printer capability characterization, bioink printability assessment, and process optimization.[28-42] Image processing can also be used for the study of reproducibility since reliable production is important in the transition from research

to industrial application, and more precisely to clinical studies.[44]

In the case of *in situ* process monitoring, even fewer studies have used image analysis to obtain layer-wise information in grid-like printing considering non-industrial devices.[28,30,35-42] Most of the approaches used top-view imaging, while some others considered also the lateral perspective to oversee the height of the printed scaffold.[36,37] Additional work was done to emphasize the role of *in situ* monitoring to investigate the influence of the rheological properties and printing parameters on the shape of the 3D-printed lines.[30] A different approach was used by Wang et al.[35] and Yang et al.[38] with the use of optical coherence tomography (OCT) to acquire high-resolution images of hydrogel scaffolds with the aim of accurately quantifying relevant morphological parameters (pore size, pore shape, surface area, porosity, and interconnectivity) for non-destructive geometric assessment and characterization of printed scaffolds. Jin et al. obtained pictures of separate layers to observe rough surfaces, fractured lines, and irregular abnormalities.[39] Eventually, Armstrong et al.[40-42] contributed significantly to the literature showing how laser scanners can be used for monitoring the nozzle trajectory and the filament width in extrusion-based 3D printing, fostering some possible solutions for *in situ* in-line feedback control. Also in our previous work, we used a camera operating in the visible to acquire images from above a construct for the identification of drift processes affecting EBB.[28]

Many of those presented works, however, suffer from the typical limitations of approaches operating in the field of visible light, namely the difficulty in discerning between target and background when they present very similar features or when, as in the case of bioinks, they are completely transparent, a feature that is very common and also essential to enable biological readouts and microscopic inspections of bioprinted constructs.

As far as we know, Moncal et al.[45] are the only ones in the literature proposing to use a thermal camera in bioprinting. However, this study has a quite different perspective compared with the one proposed in our study. In fact, Moncal et al. propose the use of thermal imaging to thermally control the extrusion process and ensure the appropriate temperatures of the printbed and printhead for promoting crosslinking for thermoresponsive hydrogels. In other words, thermal imaging is used in this study to measure the local temperature during the extrusion process.

The aim of this paper is to propose a novel solution that can overcome the previously mentioned limits of *in situ* monitoring and in-line defect detection in bioprinting when visible-range imaging is assumed. In fact, we propose the use of infrared (IR) thermal imaging for *in situ* inspection and monitoring of multi-layered 3D-bioprinted constructs. This solution is specifically suitable for transparent bioinks, where images in the visible range make edge detection hard to be implemented to detect local defects and severe deviation from the nominal shape. In this case, thermal imaging allows a clear identification of the printed geometry, which is usually deposited at a different temperature with respect to the underneath layer. This thermal signature is exploited to identify and reconstruct the printed geometry.

As a second main advantage, the thermal-based *in situ* monitoring can be used to identify defects arising on the last printed layer only. In fact, by exploiting the thermal differences between layers, the last printed layer geometry can be easily distinguished from the shapes printed on the underlying layers. Again, this capability can be hardly obtained with top-view imaging in the visible range, which allows one to obtain at each location the cumulative effect of the materials printed on different layers.

Our novel solution opens new opportunities for detecting different possible defects, such as uneven depositions and shape deviations with respect to the nominal pattern, which may arise during the bioprinting process. The proposed monitoring system based on thermal imaging would fit in the context of advanced manufacturing solutions, improving the digitization of processes and systems, the management of "Big Data," and the fusion/integration of information from multiple sensors. It would also open the opportunity to develop a process control system, to modify control inputs to correct errors in subsequent layers. Such an approach could be used not only to study geometry as has been done in this work but also to study the thermal history of thermoresponsive materials[46-48] widely used in this field. This would be a key contribution to defining a new method to quantitatively evaluate the accuracy of printed constructs and improve their quality.

The paper is structured as follows: In section 2, the biomaterials and the monitoring system used are described. In section 3, the preliminary results of such an approach are herein presented. In section 4, critical issues and advantages of this innovative approach are discussed. Finally, the main conclusions are drawn in section 5.

## 2. Materials and methods

### 2.1. Biomaterials

Two different test campaigns were conducted. In the first one, the capability of inspecting the extrusion process with thermal imaging was firstly tested without cells and considering a commercial bioink, namely CELLINK Bioink

(CELLINK, Gothenburg, Sweden), that is composed of non-animal-derived polysaccharide components, alginate, and highly hydrated cellulose nanofibrils. It is a transparent bioink selected for its consistent and temperature-independent shear-thinning properties and its similarity to the extracellular matrix, both morphological and biological.

In the second experimental campaign, bioprinting was carried out by combining the neonatal human dermal fibroblasts (nHDF; PromoCell, Heidelberg, Germany) with a custom-made alginate-gelatin hydrogel (8% w/v for both components), to test the capability of the approach of expanding its usefulness on different biomaterial and process conditions. The alginate-gelatin hydrogel represents a water-rich network of hydrophilic polymers that absorb water while maintaining their physical structure. This bioink reaches a liquid state at a temperature of 30°C and due to the presence of gelatin shows a shear-thinning behavior and undergoes gelation below room temperature, forming a gel starting from a liquid state.

### 2.2. Cell culture

nHDFs were used for bioprinting experiments. For expansion, cells were plated in T75 flasks at a seeding density of $3 \times 10^4$ cells/cm$^2$ in 15 mL of PromoCell Fibroblasts Growth Medium and then incubated at 37°C (with 5% $CO_2$). For bioink preparation, the volume of cell suspension needed for the desired cell count was centrifuged at 220 rpm for 3 min at 37°C. The resulting pellet was resuspended and manually mixed in a 1:9 ratio with the tested hydrogel. The bioink was prepared with a cell concentration of $1 \times 10^6$ cells/mL.

Given the interest of our work in the technological innovation represented by the use of a thermal imaging camera for *in situ* monitoring, no viability tests or follow-up activities of the bioprinted constructs were carried out. The cellular component was introduced inside the hydrogels in order to monitor the extrusion process of a bioink whose printing properties were representative of the process under investigation, and thus with the rheological properties of the hydrogels considered modified by the presence of the cell suspension.

### 2.3. Bioprinting set-up

The process monitoring method was applied to a pneumatic extrusion-based bioprinter, the BIO X (CELLINK, Gothenburg, Sweden), that was used to fabricate biocompatible scaffolds suitable for cells.

For the current work, general-purpose sterile high-precision conical bioprinting nozzles with a nozzle internal diameter of 0.41 (22 G) mm and a 32 mm conical nozzle length were used. For the first campaign, according to the manufacturer's indications to obtain the best printability for the selected bioink, pressure and print speed were set at 11 kPa and 20 mm/s respectively. For the second campaign, due to the custom-made nature of the bioink, after several calibration sessions, for optimal printing, the pressure and speed parameters were set at 7 kPa and 14 mm/s, respectively.

The printbed and printhead temperatures were fixed at 20°C and 30°C, respectively, for all experimentations. For the second campaign, the printbed temperature acted also as a thermal crosslinker for gelatin in the alginate–gelatin hydrogels. Printed constructs were then ionically crosslinked at the end of the printing process by dropping on them a solution of calcium chloride ($CaCl_2$).

### 2.4. 3D models

Square lattice patterns (20% infill density), commonly used in the EBB, were chosen as printing samples. At first, models of $10 \times 10 \times 1.6$ mm were chosen (Figure 1). The 3D models in STL format were created on SolidWorks software (Dassault Systèmes SE, Vélizy-Villacoublay, France).

In the first campaign, the same square lattice pattern was repeated on each layer. In the second experimental campaign, i.e., combining bioink with the nHDF, we used a different test where a different geometry was used at each layer to produce a scaffold of $14 \times 14 \times 1.6$ mm (the "step" model), just to show the impact of a temperature-based reconstruction of the geometry, which allows in principle to observe/monitor the geometry of the last layer only.

In order to produce this second model of interest, the G-code was modified using NC Viewer, an online open-source G-code programming application to obtain a model where only a partial portion of the layer was printed at layers 2, 3, and 4, as shown in Figure 2.

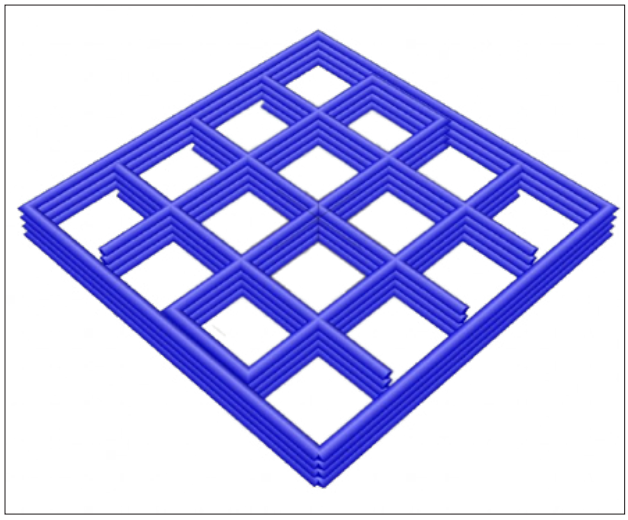

**Figure 1.** 3D representation of the standard model.

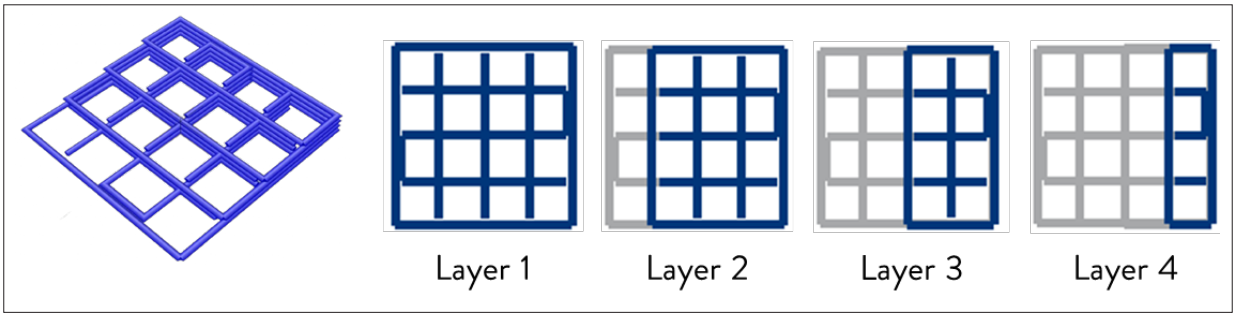


**Figure 2.** 3D and sliced layers representation of the "steps" model.

In all the experimental campaigns, Slic3r software (a free 3D slicing engine software for 3D printers) was used for slicing the STL models.

### 2.5. Process sensing

The apparatus for monitoring the bioprinted geometries consists of the following components:

(i) A visible-range (VR) camera. The first sensing equipment is an integrated camera (1600 × 1200 pixels), which is already mounted on the bioprinter on one of the three available heads and is thus able to acquire *in situ* co-axial HD images after each printed layer.

(ii) An infrared-range (IR) camera. This second sensing system is a high-frequency thermal camera, namely a mid-wave infrared indium antimonide thermocamera (temperature sensibility ±1°C, 640 × 512 pixels) for video detection, the FLIR X6900sc MWIR (FLIR® Systems Inc., Wilsonville, US), allowing acquisition of *in situ* off-axis IR images.

As the second camera can acquire images at high frequency, the whole printing process was recorded continuously using an optic with focal distances of 25 mm, which led to an image resolution of 200 µm/pixel (Figure 3). This resolution is quite low and was the effect of considering our existing camera, usually used for monitoring other AM processes (namely powder bed fusion processes). However, as this study was just designed to prove the feasibility of a new sensing architecture for geometrical reconstruction, we did not decide to acquire a new ad-hoc thermal sensing appropriately focusing on EBB. Significant improvements in the current results are currently observed using an IR camera and optics specifically selected for EBB processes.

The camera was previously calibrated in a temperature range between 0°C and 150°C, with an accuracy of 1°C. Videos were acquired with a frequency of 30 fps. The acquisition frequency has to be sufficiently high to notice the temperature change. Before the acquisition, during the calibration phase, fiducial points were also marked on a sample of graph paper placed on the printbed at the acquisition target area, for further registration operations.

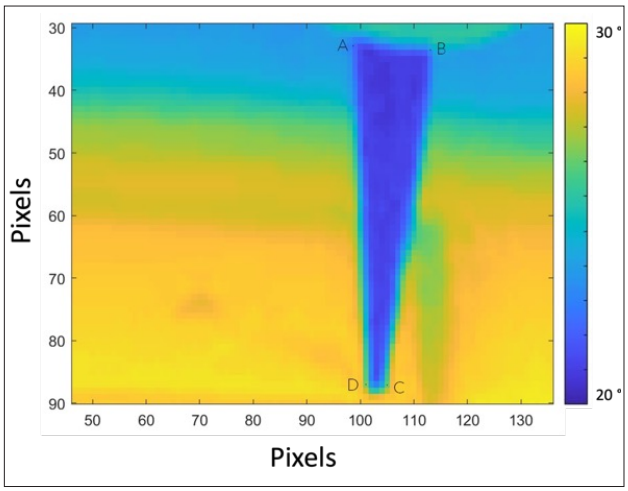


**Figure 3.** Image resolution sensibility for the 25 mm optic. The nozzle with a diameter of 0.41 mm (22 G) and a conical length of 32 mm was used as the calibration target.

The image acquisition environment conditions tested are shown in Figure 4.

Temperature data were exported using ExaminIR software (FLIR® Systems Inc., Wilsonville, USA), and then post-processed with different custom-made Matlab® R2020b (MathWorks, Natick, USA) algorithms. The main image processing steps are briefly reviewed in the next section.

### 2.6. Layer-wise image analysis: a novel solution for thermal image processing

In this work, a custom-made algorithm was developed, optimized, and tested on images gathered with the two different cameras (the VR and IR images). The algorithm was applied to images gained at each layer. The image processing was based on custom-made methods of image rectification (roto translation), segmentation, and binarization (Figure 5). Cropping was also used to focus on the region of interest. Only crop and rotation were applied

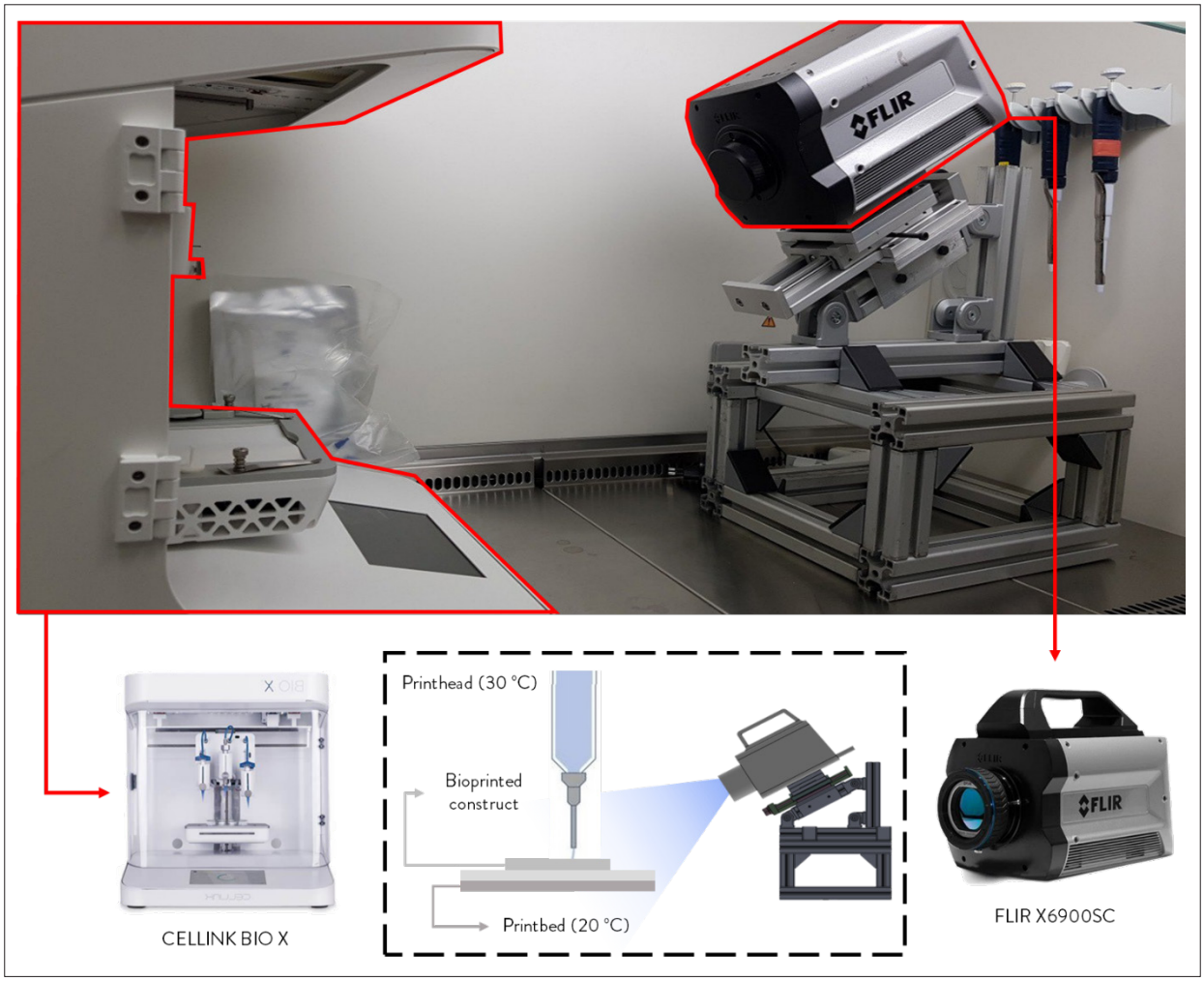


**Figure 4.** Monitoring system and printbed acquisition scheme. Under normal circumstances, the bioprinted construct is deposited on a sterilized substrate (glass petri dish in this case) positioned upon the printbed for better temperature control.

to VR images, as a top-view solution was available in this case. The function *mat2gray* was used for each frame of the series, to rescale the pixel intensity linearly between 0 and 1. This was done because even if HD images were characterized by an 8-bit integer value pixel-wise, the IR camera provided a radiance value on a continuous scale.

### 2.7. Bradley adaptive thresholding algorithm

Segmentation is a diverse and dynamic field within computer vision and image processing, characterized by a wide range of algorithms and approaches tailored to various applications and imaging modalities. In previous internal experimentations, we conducted extensive testing of both supervised and unsupervised algorithms, aiming to identify the most effective method for achieving reconstructions with less error in both thermal and visible image datasets. Despite the diverse algorithms employed, our analyses consistently demonstrated that image thresholding methods outperformed others in terms of quantitative metrics. Whether applied to visible or thermal images, this method consistently yielded superior results, showcasing its robustness in image reconstruction. Moreover, when considering the utility of image thresholding, particularly in the context of VR and IR images, its appeal lies in its simplicity and effectiveness. While more complex segmentation methods exist, such as region-growing, edge detection, or deep learning-based techniques, image thresholding offers a straightforward and computationally efficient solution. Thus, the choice to use image thresholding over more complex methods in this context was driven by the need for simplicity and speed.

In global thresholding, a single threshold value is applied uniformly to the entire image, which may lead to suboptimal results when dealing with images characterized by non-uniform lighting conditions or

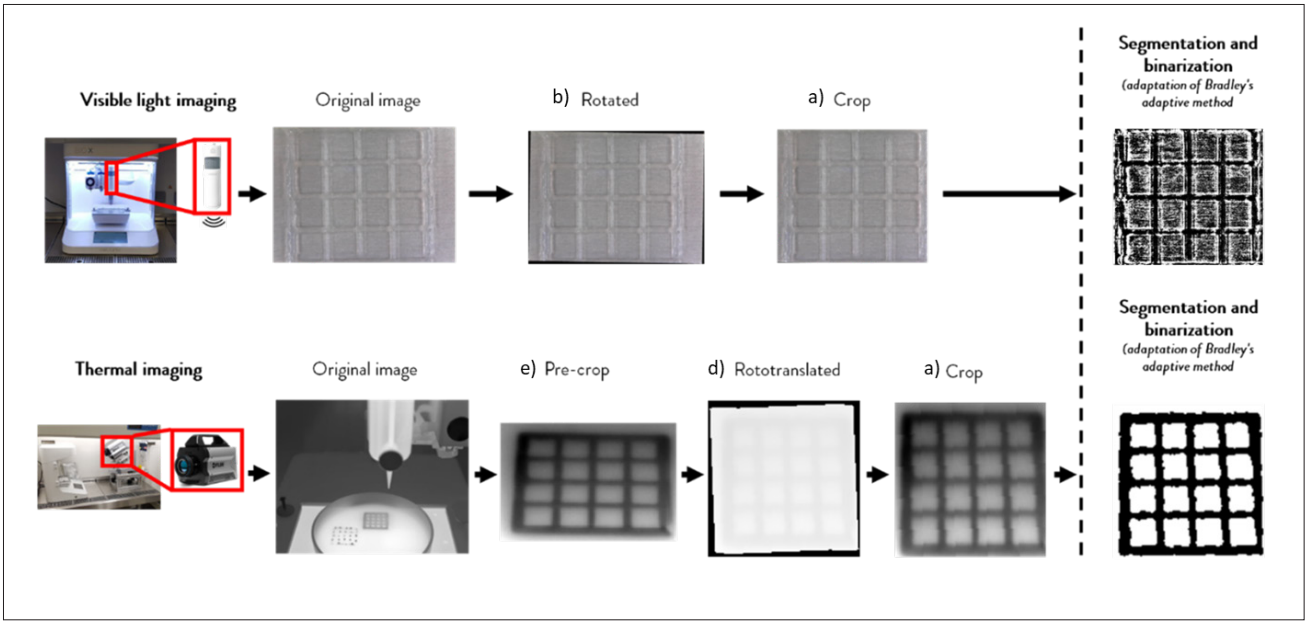


**Figure 5.** Steps of the procedure. Cropping (a) and rotation (b) and operations were applied to the VR images using MATLAB basic functions, to standardize the application of segmentation algorithms. In the case of IR images, due to the off-axis positioning of the thermal camera, the roto translation (c) operations were applied via MATLAB *fitgeotform2d* function only to the region of interest of the whole frame (d).

variations in object intensity. Adaptive thresholding, as opposed to global thresholding, offers a notable advantage in scenarios where image illumination and contrast vary across different regions such as in our VR images, or where there are variations in object intensity like in IR images, where these discrepancies are common. Adaptive thresholding addresses these challenges by determining a local threshold value for each pixel based on its immediate neighborhood. This adaptive approach allows the algorithm to account for local variations in intensity, resulting in improved segmentation accuracy and robustness. By tailoring the threshold to the specific characteristics of our images, adaptive thresholding effectively mitigates the shortcomings of global thresholding, making it a superior choice for applications where precise object delineation is paramount.

The developed algorithm consisted briefly of two steps:

(i) In the first step, the image underwent morphological opening processing for removing small noises while preserving the shape and size of larger objects with *imopen* and *imsubtract* Matlab® built-in functions. With this operation, the image was eroded and then dilated using a disk structuring element of radius $r$ with the *strel* Matlab® built-in function for both operations.

(ii) In the second step, a binary image was obtained from the pre-processed thermal image by using Bradley's "adaptive" method[49] within the *imbinarize* Matlab® built-in function. This method binarizes the image using a locally adaptive threshold. The threshold was automatically computed by *adaptthresh* Matlab® built-in function based on the local mean intensity in the neighborhood of each pixel at a given sensitivity $s$, which indicates sensitivity toward thresholding more pixels as foreground.

(iii) The radius $r$ and the sensitivity $s$ within the algorithm were chosen following a visual inspection of the quality of the segmentation process through an empirical approach. This led to $r = 20$ and $s = 0.5$.

The proposed process monitoring approach relied on a comparison between both the binarized VR images and IR images obtained with the respective nominal shape of each layer. The image registration with the nominal shape was conducted with the utilization of the landmark points previously mentioned. To accomplish this registration, we employed the "*fitgeotrans*" function within the MATLAB® software platform. This function was configured to utilize the "*nonreflectivesimilarity*" property, a transformation type well-suited for preserving shape integrity while enabling translation, rotation, and scaling adjustments. Notably, this approach ensured that the relative shapes within the moving image remained unaltered, with the primary variations being attributed to transformations preserving parallelism and straightness, thereby upholding the integrity of our comparative analysis. The comparison evaluation was conducted by calculating the Dice

similarity coefficient (DSC),[50] a well-established measure commonly employed in image analysis and medical imaging applications, between the binarized target image (VR or IR) and the relative binarized nominal shape image:

$$DSC = 2 \cdot \frac{|X \text{ I } Y|}{|X| + |Y|} \quad \text{(I)}$$

where $X$ is the set of foreground pixels in the target image and $Y$ is the corresponding set of foreground pixels in the binarized nominal shape image, respectively. The DSC value ranges between 0 and 1, where a value closer to 0 indicates less spatial overlap between regions $X$ and $Y$, while a value closer to 1 indicates a higher degree of spatial overlap. By employing this metric, we aimed to quantify the degree of similarity between the two image sets.

### 2.8. Proof-of-concept of on-line geometric reconstruction capability

Since different materials exhibit different thermal properties, during the second campaign, it was also decided to implement the developed segmentation algorithm along with a tracking algorithm, which relied on the Kanade–Lucas–Tomasi (KLT) algorithm, to perform segmentation of the deposited construct at the time of maximum thermal gradient between background and foreground (Figure 6), to enhance the monitoring capabilities of our system. For further details on algorithm implementation, we suggest the reader refer to a previous work of ours,[51] where the KLT algorithm, renowned within the field of computer vision for its effectiveness as a feature-based tracking method, showed excellent performance in the tracking of the extruder of a 3D printer across consecutive thermal video frames.

Since the extruder of our bioprinter operated under the fundamental assumptions of consistent object brightness, limited displacement, and full visibility in all video frames, it was possible to apply a similar approach to reconstruct the geometry of each layer of the "step" model, through an integration of the segmented pixel obtained frame-by-frame.

## 3. Results

### 3.1 Comparison of segmentation performance between VR and IR images

In the following, results obtained on a seven-layer construct printed in the before-mentioned conditions were used as a reference to show the promising advantage of IR images. In Figure 7, it is possible to see the images of each of the seven layers captured with the two types of cameras. Each image demonstrates the respective reconstructed geometry and the calculated DSC value. It is possible to notice that IR images led to a better geometry reconstruction, confirmed not only by visual inspection, albeit with all the relevant hardware resolution limitations, but also by the DSC values obtained, which were always higher than those obtained for VR images. Furthermore, it is possible to identify trends in the performance of the metrics in the two different sets of images.

### 3.2. Last layer detection

In the course of the experimental campaigns, several samples quite frequently suffered from printing problems, which resulted in defects on their appearance. Figure 8 shows the original VR image, the original IR image, and the IR segmented image of the third layer of a three-layer construct that, despite being printed with the same printing parameters as the other samples, ran into under-extrusion problems, presenting a "pillar" geometry in the last printed

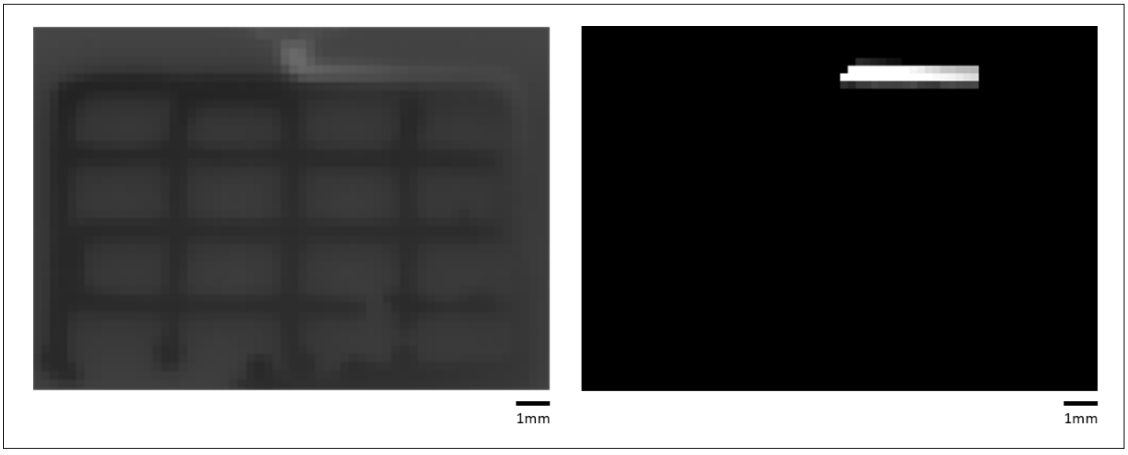


**Figure 6.** On the left, the original IR frame from a video of the second campaign. On the right frame-by-frame integration of the segmented pixel once extruded from the nozzle of the first instants of the process.

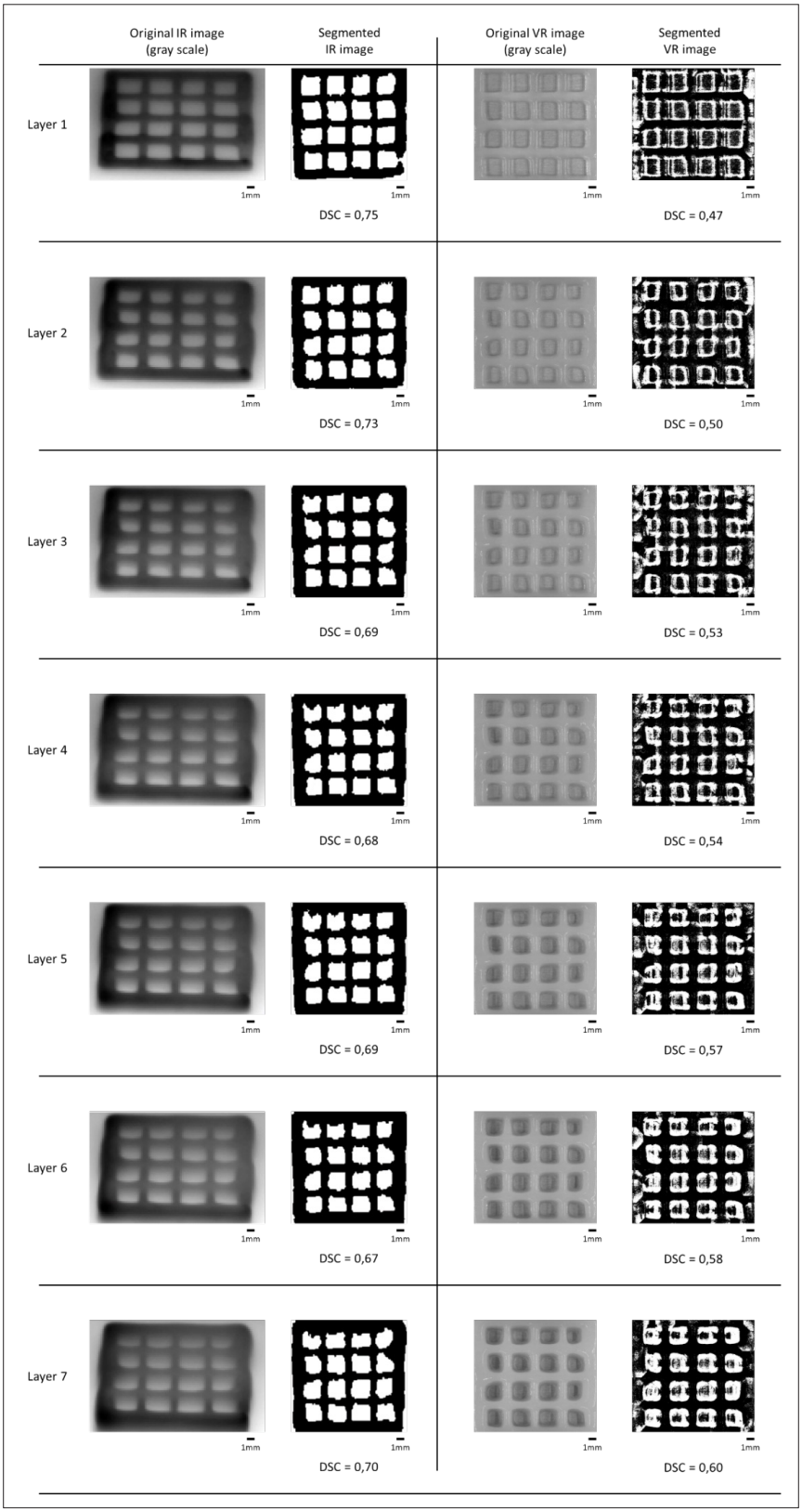


**Figure 7.** Images of each of the seven layers of the printed sample. On the left panel, there are original and segmented IR images; on the right panel, there are original and segmented VR images. For each reconstructed geometry, the DSC index is also reported.

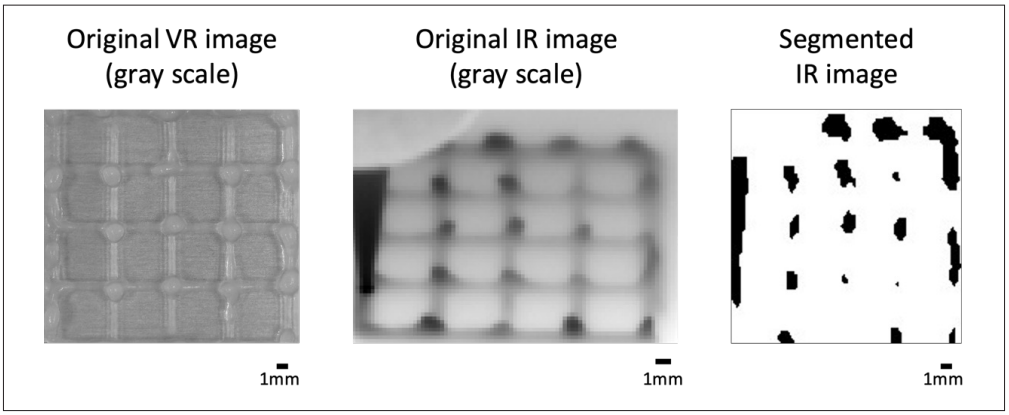


**Figure 8.** Defective layer reconstruction. From left to right: the original VR image, the original IR image, and the result of the segmentation of the IR image.

layer instead of the expected grid. It is possible to notice that the thermal imaging was able to clearly highlight the defective zones of the constructs, especially in the node where the excess of material translates in a higher temperature locally affecting the last "layer" deposited.

### 3.3. Proof-of-concept of in-line geometric reconstruction capability

Despite the limitations due to the resolution of the acquisition system in our possession, it is possible to see the outcomes of the extruder tracking process, as shown in Figure 9, where only the first three layers of a sample are shown as an example. It can be seen that the IR images allowed the reconstruction of the geometry of individual layers also with a transparent bioink with fast thermal kinetics. This would have been quite hard with VR cameras since due to the transparency of the bioink it would not have been possible to discern the background from the foreground as previously demonstrated.

## 4. Discussion

The work here presented describes a simple monitoring experiment in which the feasibility of using thermal imaging for geometry detection of printed constructs was demonstrated. The literature did not provide any previous examples of utilizing thermographic imaging for the geometric analysis of bioprinting constructs. However, the employed thermographic imaging device successfully captured thermal image sequences of bioprinting experiments, allowing for *in situ* analysis and evaluation of the geometric characteristics of the constructs. More specifically, we have demonstrated the effectiveness in being able to discriminate qualitatively between different layers because of the differences in temperature between them. Having set the temperature of the printhead at 30°C and of the printbed at 20°C has created a temperature gradient typical for this type of process, in which temperatures must be guaranteed at the same time to ensure good printability characteristics of the materials and also cell survival. The fine identification of this temperature difference was granted by the high sensitivity of the thermal imaging camera used.

Among the reviewed literature, only Wang et al.[34] presented their experimental design method utilizing a cell-loaded bioink. Despite the fact that most of the *in situ* methods were theoretically applicable to working with cells, Wang et al. were the only ones to demonstrate its practical implementation. One of the major challenges in utilizing a cell-loaded bioink was ensuring sterile conditions throughout the bioprinting experiments and process monitoring. Our proposed method exploits IR radiation to overcome the limitations of systems and devices operating in visible light (such as the VR camera used in this work) since they would not be affected by the ambient brightness and transparency conditions of the bioink.

The capability to identify and segment the deposited bioink filament in real time allowed for the measurement of filament width at every time instant during the printing process. Previous studies by Yang et al.[34] and Armstrong et al.[40-42] characterized the filament width in *in situ* bioprinting experiments, but they utilized more viscous and opaque bioinks compared to the transparent alginate-gelatin hydrogel used in this work. The viscosity of the bioink affects the distinguishability of different layers on the *Z*-axis. Additionally, the previous studies employed simplified layer designs without intersections or adjacent filaments, whereas this work demonstrated the technique with layered constructs featuring grid patterns. Consequently, filament quality characteristics were assessed even at intersections and when a filament was printed close to a previously deposited one, thanks to the distinguishability of hot bioink from cold bioink using thermal imaging.

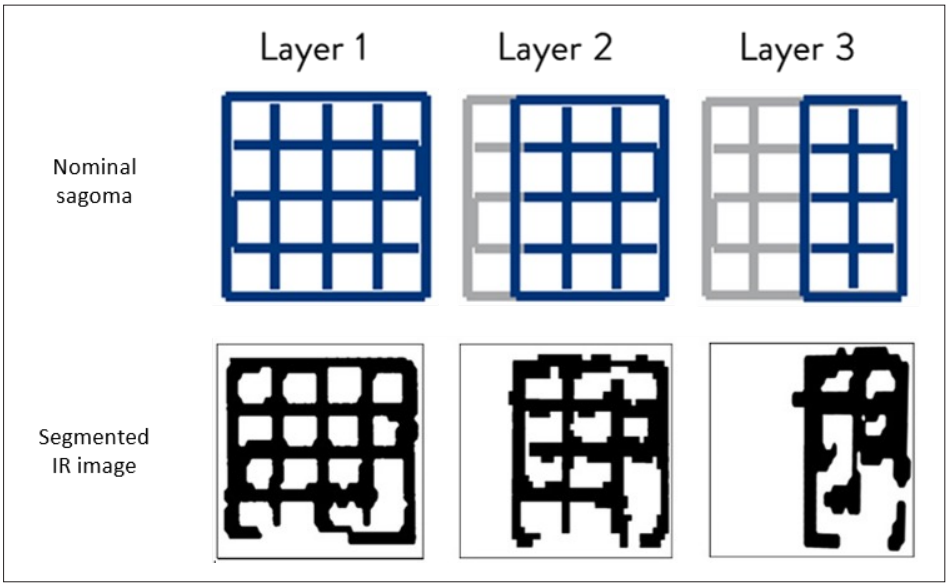


**Figure 9.** Geometric reconstruction from tracking approach outcomes. Top row shows the nominal sagoma images of the first three layers of a construct (highlighted in blue). Bottom row shows the respective reconstructed layers obtained from the application of our algorithm during the tracking process.

The capability to segment the bioink filament at each moment in the 3D printing process provides a unique advantage: the reconstruction of the distinct profile of each individual layer, isolated from the layers beneath or the substrate. This is especially crucial when dealing with transparent bioink. Traditional visible range images encounter challenges in distinguishing between multiple layers deposited on top of each other. This issue becomes particularly pronounced when transparent bioink is employed, as the cumulative effect of all printed layers results in an overall image that combines these layers. Consequently, the visual representation becomes a summation of all the printed layers, obscuring the details of individual layers and compromising the ability to discern their distinct characteristics.[30] In contrast, the developed method could isolate the bioink belonging to a layer printed on top of a previous one, effectively separating it from the rest of the printed construct. It is important to note that the proposed method considers the shape of the bioink at the moment of deposition and does not account for spreading or diffusion that may occur between material deposition and image acquisition. This distinction is evident in VR images where certain pores may appear occluded while being open in the thermal reconstruction of the equivalent layer.

Upon reconstructing the profile of a layer, the developed method enabled the evaluation of its geometric accuracy. The DSC was assessed by measuring the similarity between the reconstructed profile and the binarized image of the corresponding nominal layer. Of course, this method is not exempt from limitations. Monitoring devices in the IR field have a higher purchase price. They are advanced devices built with complicated components, and in the case of IR devices, their purchase prices are higher than those in visible light. Optics and detection systems in the IR are not as widely used as those in VR. These components are more expensive, thus increasing the initial cost. Moreover, thermal images cannot be captured if certain materials, such as water and glass, are used. Unlike VR, IR radiation cannot pass through water or glass, from which it is reflected as in a mirror, unless special arrangements are made, such as the use of special filters or windows made of materials that allow the radiation to be transmitted without interference. In addition, the monitoring system can only be used in printing processes where the geometry of the last printed layer (or the construct in general) can be captured by registration systems (not applicable in SLA bioprinting, for example, unless custom-made systems are foreseen at the machine design stage).

Despite these limitations, this approach would also open the opportunity to develop a process control system and to modify control inputs for correcting errors in subsequent layers. It is recommended that the approach be followed both by the end-users of extrusion bioprinters and the manufacturer of bioprinters, since the monitoring system like the one proposed can be implemented also in the machines already on the market without having to create new bioprinters integrated with this system.

For future development, a better image processing system capable of identifying more features and operating in real-time should be developed. *In situ* monitoring techniques incorporated with the feedback systems for process control should also be implemented.

## 5. Conclusion

In conclusion, this study has introduced a novel approach for monitoring bioprinted constructs using thermal imaging, demonstrating its feasibility and effectiveness. The absence of previous instances employing thermographic imaging for the geometric analysis of bioprinting constructs emphasizes the innovative nature of this work. The successful capture of thermal image sequences in real-time using the employed thermographic imaging device allowed for *in situ* assessment of construct's geometrical characteristics. Specifically, the method highlighted the ability to qualitatively distinguish between different layers based on their temperature disparities.

Our method effectively overcomes limitations posed by visible light systems in discerning bioink layers, particularly in transparent bioinks. The method's capacity to segment deposited bioink filaments in real time enables the measurement of filament width during the printing process. Additionally, the technique permitted the isolation and separate reconstruction of individual layer profiles, addressing the challenge of layer superposition.

In summary, the application of thermal imaging technology to construct bioprinting represents an innovative step toward enhancing process monitoring and quality control, laying the foundation for further advancements in bioprinting technology and its industrial implementation.

## Acknowledgments

None.

## Funding

This research was partially funded by the European Commission under the "HORIZON-CL4-2021-DIGITAL-EMERGING-01 project BioProS - Biointelligent Production Sensor to Measure Viral Activity" (grant agreement no. 101070120, 2022–2026).

## Conflict of interest

The authors declare no conflicts of interest.

## Author contributions

*Conceptualization:* Bianca Maria Colosimo, Davide Moscatelli, Simone Giovanni Gugliandolo
*Data curation:* Simone Giovanni Gugliandolo
*Formal analysis:* Simone Giovanni Gugliandolo, Egon Prioglio
*Investigation:* Simone Giovanni Gugliandolo, Egon Prioglio
*Methodology:* Bianca Maria Colosimo, Simone Giovanni Gugliandolo, Egon Prioglio
*Supervision:* Bianca Maria Colosimo, Davide Moscatelli
*Writing – original draft:* Simone Giovanni Gugliandolo, Bianca Maria Colosimo
*Writing – review & editing:* Bianca Maria Colosimo, Davide Moscatelli

## Ethics approval and consent to participate

Not applicable.

## Consent for publication

Not applicable.

## Availability of data

Data are available from the corresponding author upon reasonable request.

## References

1. Moroni L, Boland T, Burdick JA, et al. Biofabrication: a guide to technology and terminology. *Trends Biotechnol*. 2018;36(4):384-402. doi: 10.1016/j.tibtech.2017.10.015
2. Ng WL, Chua CK, Shen YF. Print me an organ! Why we are not there yet. *Prog Polym Sci*. 2019;97:101145. doi: 10.1016/j.progpolymsci.2019.101145
3. Santoni S, Gugliandolo SG, Sponchioni M, Moscatelli D, Colosimo BM. 3D bioprinting: current status and trends—a guide to the literature and industrial practice. *Bio-Des Manuf*. 2021;5(1):14-42. doi: 10.1007/S42242-021-00165-0
4. Pereira FDAS, Parfenov V, Khesuani YD, Ovsianikov A, Mironov V. Commercial 3D bioprinters. In: Ovsianikov A, Yoo J, Mironov V, eds. *3D Printing and Biofabrication*. Cham: Springer; 2018: 535-549. doi: 10.1007/978-3-319-45444-3_12
5. Jang J, Park JY, Gao G, Cho D-W. Biomaterials-based 3D cell printing for next-generation therapeutics and diagnostics. *Biomaterials*. 2018;156:88-106. doi: 10.1016/j.biomaterials.2017.11.030
6. Constante G, Apsite I, Alkhamis H, et al. 4D biofabrication using a combination of 3D printing and melt-electrowriting of shape-morphing polymers. *ACS Appl Mater Interfaces*. 2021;13(11):12767-12776. doi: 10.1021/acsami.0c18608
7. Caleffi JT, Aal MCE, Gallindo H de OM, et al. Magnetic 3D cell culture: state of the art and current advances. *Life Sci*. 2021;286:120028. doi: 10.1016/j.lfs.2021.120028
8. Hu X, Zheng J, Hu Q, et al. Smart acoustic 3D cell construct assembly with high-resolution. *Biofabrication*. 2022;14(4). doi: 10.1088/1758-5090/ac7c90

9. Moldovan NI, Hibino N, Nakayama K. Principles of the kenzan method for robotic cell spheroid-based three-dimensional bioprinting. *Tissue Eng Part B Rev*. 2017;23(3):237-244. doi: 10.1089/ten.teb.2016.0322
10. Zhou X, Wu H, Wen H, Zheng B. Advances in single-cell printing. *Micromachines*. 2022;13(1):80. doi: 10.3390/mi13010080
11. Ramesh S, Harrysson OLA, Rao PK, et al. Extrusion bioprinting: recent progress, challenges, and future opportunities. *Bioprinting*. 2021;21:e00116. doi: 10.1016/j.bprint.2020.e00116
12. Boularaoui S, Al Hussein G, Khan KA, Christoforou N, Stefanini C. An overview of extrusion-based bioprinting with a focus on induced shear stress and its effect on cell viability. *Bioprinting*. 2020;20:e00093. doi: 10.1016/J.BPRINT.2020.E00093
13. Saunders RE, Derby B. Inkjet printing biomaterials for tissue engineering: bioprinting. *Int Mater Rev.* 2014;59(8):430-448. doi: 10.1179/1743280414Y.0000000040
14. Ng WL, Huang X, Shkolnikov V, Suntornnond R, Yeong WY. Polyvinylpyrrolidone-based bioink: influence of bioink properties on printing performance and cell proliferation during inkjet-based bioprinting. *Bio-Des Manuf*. 2023;6(6):676-690. doi: 10.1007/S42242-023-00245-3/FIGURES/5
15. Levato R, Dudaryeva O, Garciamendez-Mijares CE, et al. Light-based vat-polymerization bioprinting. *Nat Rev Methods Primers*. 2023;3(1):1-19. doi: 10.1038/s43586-023-00231-0
16. Gao G, Kim BS, Jang J, Cho D-W. Recent strategies in extrusion-based three-dimensional cell printing toward organ biofabrication. *ACS Biomater Sci Eng*. 2019;5(3):1150-1169. doi: 10.1021/acsbiomaterials.8b00691
17. Antoshin AA, Churbanov SN, Minaev NV, et al. LIFT-bioprinting, is it worth it? *Bioprinting*. 2019;15(May):e00052. doi: 10.1016/j.bprint.2019.e00052
18. Nuñez Bernal P, Delrot P, Loterie D, et al. Volumetric bioprinting of complex living-tissue constructs within seconds. *Adv Mater.* 2019;31(42):1904209. doi: 10.1002/ADMA.201904209
19. Kumar H, Kim K. Stereolithography 3D bioprinting. *Methods Mol Biol*. 2020;2140:93-108. doi: 10.1007/978-1-0716-0520-2_6
20. Sheth R, Balesh ER, Zhang YS, Hirsch JA, Khademhosseini A, Oklu R. Three-dimensional printing: an enabling technology for IR. *J Vasc Interv Radiol*. 2016;27(6):859-865. doi: 10.1016/j.jvir.2016.02.029
21. Bouguéon G, Kauss T, Dessane B et al., 2019, Micro- and nano-formulations for bioprinting and additive manufacturing. Drug Discov Today 24 (1): 163–178. doi: 10.1016/j.drudis.2018.10.013
22. Caltanissetta F, Grasso M, Petrò S, Colosimo BM. Characterization of in-situ measurements based on layerwise imaging in laser powder bed fusion. *Addit Manuf*. 2018;24:183-199. doi: 10.1016/J.ADDMA.2018.09.017
23. Grasso M, Remani A, Dickins A, Colosimo BM, Leach RK. In-situ measurement and monitoring methods for metal powder bed fusion: an updated review. *Meas Sci Technol*. 2021;32(11):112001. doi: 10.1088/1361-6501/AC0B6B
24. Grasso M, Colosimo BM. Process defects and in situ monitoring methods in metal powder bed fusion: a review. *Meas Sci Technol*. 2017;28(4):044005. doi: 10.1088/1361-6501/AA5C4F
25. Colosimo BM, Huang Q, Dasgupta T, Tsung F. Opportunities and challenges of quality engineering for additive manufacturing. *J Qual Technol.* 2018;50(3):233-252. doi: 10.1080/00224065.2018.1487726
26. AbouelNour Y, Gupta N. Assisted defect detection by in-process monitoring of additive manufacturing using optical imaging and infrared thermography. *Addit Manuf*. 2023;67:103483. doi: 10.1016/J.ADDMA.2023.103483
27. Hossain REN, Lewis J, Moore AL. In situ infrared temperature sensing for real-time defect detection in additive manufacturing. *Addit Manuf*. 2021;47:102328. doi: 10.1016/J.ADDMA.2021.102328
28. Gugliandolo SG, Margarita A, Santoni S, Moscatelli D, Colosimo BM. In-situ monitoring of defects in extrusion-based bioprinting processes using visible light imaging. *Procedia CIRP*. 2022;110(C):219-224. doi: 10.1016/J.PROCIR.2022.06.040
29. Schmieg B, Gretzinger S, Schuhmann S, Guthausen G, Hubbuch J. Magnetic resonance imaging as a tool for quality control in extrusion-based bioprinting. *Biotechnol J*. 2022;17(5):2100336. doi: 10.1002/BIOT.202100336
30. Strauß S, Meutelet R, Radosevic L, Gretzinger S, Hubbuch J. Image analysis as PAT-tool for use in extrusion-based bioprinting. *Bioprinting*. 2021;21:e00112. doi: 10.1016/J.BPRINT.2020.E00112
31. Uzun-Per M, Gillispie GJ, Tavolara TE, et al. Automated image analysis methodologies to compute bioink printability. *Adv Eng Mater*. 2021;23(4):2000900. doi: 10.1002/ADEM.202000900
32. Bone JM, Childs CM, Menon A, et al. Hierarchical machine learning for high-fidelity 3D printed biopolymers. *ACS Biomater Sci Eng*. 2020;6(12):7021-7031. doi: 10.1021/acsbiomaterials.0c00755
33. Sedigh A, DiPiero D, Shine KM, Tomlinson RE. Enhancing precision in bioprinting utilizing fuzzy systems. *Bioprinting*. 2022;25:e00190. doi: 10.1016/J.BPRINT.2021.E00190

34. Wang L, Xu ME, Luo L, Zhou Y, Si P. Iterative feedback bio-printing-derived cell-laden hydrogel scaffolds with optimal geometrical fidelity and cellular controllability. *Sci Rep*. 2018;8(1):1-13.
doi: 10.1038/s41598-018-21274-4

35. Wang L, Xu M, Zhang L, Zhou Q, Luo L. Automated quantitative assessment of three-dimensional bioprinted hydrogel scaffolds using optical coherence tomography. *Biomed Opt Express*. 2016;7(3):894.
doi: 10.1364/boe.7.000894

36. Bonatti AF, Vozzi G, Chua CK, De Maria C. A deep learning approach for error detection and quantification in extrusion-based bioprinting. *Mater Today Proc*. 2022;70:131-135.
doi: 10.1016/J.MATPR.2022.09.006

37. Bonatti AF, Vozzi G, Chua CK, De Maria C. A deep learning quality control loop of the extrusion-based bioprinting process. *Int J Bioprint*. 2022;8(4):307-320.
doi: 10.18063/IJB.V8I4.620

38. Yang S, Chen Q, Wang L, Xu M. In situ defect detection and feedback control with three-dimensional extrusion-based bioprinter-associated optical coherence tomography. *Int J Bioprint*. 2022;9(1):47-62.
doi: 10.18063/IJB.V9I1.624

39. Jin Z, Zhang Z, Shao X, Gu GX. Monitoring anomalies in 3D bioprinting with deep neural networks. *ACS Biomater Sci Eng*. 2023;9(7):3945-3952.
doi: 10.1021/acsbiomaterials.0c01761

40. Armstrong AA, Alleyne AG, Wagoner Johnson AJ. 1D and 2D error assessment and correction for extrusion-based bioprinting using process sensing and control strategies. *Biofabrication*. 2020;12(4):045023.
doi: 10.1088/1758-5090/ABA8EE

41. Armstrong AA, Norato J, Alleyne AG, Johnson AJW. Direct process feedback in extrusion-based 3D bioprinting. *Biofabrication*. 2019;12(1):015017.
doi: 10.1088/1758-5090/AB4D97

42. Armstrong AA, Pfeil A, Alleyne AG, Johnson AJW. Process monitoring and control strategies in extrusion-based bioprinting to fabricate spatially graded structures. *Bioprinting*. 2021;21:e00126.
doi: 10.1016/J.BPRINT.2020.E00126

43. Gao T, Gillispie GJ, Copus JS, et al. Optimization of gelatin-alginate composite bioink printability using rheological parameters: a systematic approach. *Biofabrication*. 2018;10(3):034106.
doi: 10.1088/1758-5090/aacdc7

44. Yaneva A, Shopova D, Bakova D, et al. The progress in bioprinting and its potential impact on health-related quality of life. *Bioengineering*. 2023;10(8):910.
doi: 10.3390/BIOENGINEERING10080910

45. Moncal KK, Ozbolat V, Datta P, Heo DN, Ozbolat IT. Thermally-controlled extrusion-based bioprinting of collagen. *J Mater Sci Mater Med*. 2019;30:55.
doi: 10.1007/s10856-019-6258-2

46. Santoni S, Sponchioni M, Gugliandolo SG, Colosimo BM, Moscatelli D. Preliminary tests on PEG-based thermoresponsive polymers for the production of 3D bioprinted constructs. *Procedia CIRP*. 2022;110(C): 350-355.
doi: 10.1016/j.procir.2022.06.062

47. Suntornnond R, An J, Chua CK. Bioprinting of thermoresponsive hydrogels for next generation tissue engineering: a review. *Macromol Mater Eng*. 2017;302(1):1600266.
doi: 10.1002/mame.201600266

48. Hsieh FY, Lin HH, Hsu S-H. 3D bioprinting of neural stem cell-laden thermoresponsive biodegradable polyurethane hydrogel and potential in central nervous system repair. *Biomaterials*. 2015;71:48-57.
doi: 10.1016/j.biomaterials.2015.08.028

49. Bradley D, Roth G. Adaptive thresholding using the integral image. *J Graph Tools*. 2007;12(2):13-21.
doi: 10.1080/2151237X.2007.10129236

50. Dice LR. Measures of the amount of ecologic association between species. *Ecology*. 1945;26(3):297-302.
doi: 10.2307/1932409

51. Caltanissetta F, Dreifus G, Hart AJ, Colosimo BM. In-situ monitoring of material extrusion processes via thermal videoimaging with application to big area additive manufacturing (BAAM). *Addit Manuf*. 2022;58:102995.
doi: 10.1016/J.ADDMA.2022.102995